Ocean Dynamics (2020) 70:1587–1601
https://doi.org/10.1007/s10236-020-01415-y

Case studies on the parameterization schemes of sea ice fragmentation for ocean waves

Xiying Liu [1,2] · Guanghong Liao [1,2] · Chenchen Lu [3]

Received: 10 November 2019 / Accepted: 24 September 2020 / Published online: 24 October 2020

Abstract
Sea ice on the Southern Ocean has large seasonal variations. Floe size distribution has an important influence on the dynamic and thermodynamic processes of sea ice in the region with large seasonal variation and the Marginal Ice Zone. In the work, we introduced a prognostic floe size distribution (FSD) into a sea ice model and improved the calculation of lateral melt of sea ice. On this basis, we implemented two schemes of sea ice fragmentation for ocean waves and performed case studies on the effects of swell fracture on Antarctic sea ice variations. From the studies, we show it that the two schemes of sea ice fragmentation have unique characteristics in the mass transfer of sea ice among the floe size categories; if the break-up of ice floe is neglected, the effect of the improvement in lateral melt rate calculation on sea ice simulation is not significant; the simulated patterns of reduced sea ice concentration in March because of the effects of sea ice fragmentation and modification in calculation of lateral melt rate are similar since the two schemes of sea ice fragmentation both have close connections with sea ice thickness; the simulated sea ice area fraction for individual floe size categories varies with sea ice fragmentation schemes; this is due to their difference in characteristics of sea ice mass transfer among the floe size categories.

Keywords Swell fracture · Numerical modeling · Floe size distribution · Sea ice · Antarctic

1 Introduction

Climate change is a major crisis and severe challenge facing mankind and has become the focus of common concerns of countries around the world. Sea ice is not only a component of the climate system but also an indicator of climate change. Its change is one of the most important factors affecting the prediction of climate change (Laxon et al. 2003). Under the background of global warming, both the sea ice concentration and the duration of sea ice coverage experience rapid change (Stammerjohn et al. 2012; Lang et al. 2017). Studies suggest that the floe size distribution (FSD) of sea ice is a potential factor controlling the change rate of sea ice on a global scale (Toyota et al. 2016).

In marginal ice zone (MIZ, referring to the boundary between the open sea and the region covered by sea ice. In MIZ, the dynamic characteristics of sea ice are significantly affected by the processes of open sea) and area with large seasonal variation in sea ice, sea ice has the characteristics of discrete distribution and strong mobility (Zhang et al. 2012; Vihma et al., 2014). The characteristics of the floe size of sea ice in these regions differ from those in the perennial ice zone. FSD has an important influence on the dynamic and thermodynamic processes of sea ice: the exchange of momentum between air and sea ice varies with the floe size; ice floe with specific size is more susceptible to break-up due to ocean wave (Dumont et al. 2011); the melt rate of sea ice depends on the floe size, and the smaller the size of ice floe, the bigger the lateral melt rate (Soh et al. 1998); in addition, FSD and the shape of ice floe may provide clues for understanding the formation process of ice floe (Steele 1992); as mentioned before, FSD is a potential factor to control the variation rate of sea ice extent on a global scale (Toyota et al. 2016). In MIZ, the shape of ice floes are varied (Dumont et al. 2011), the influence of wind stirring is strong, and the effect of ice

Responsible Editor: Fanghua Xu

This article is part of the Topical Collection on the *11th International Workshop on Modeling the Ocean (IWMO), Wuxi, China, 17-20 June 2019*

✉ Xiying Liu
xyliu@hhu.edu.cn

[1] Key Laboratory of Ministry of Education for Coastal Disaster and Protection, Hohai University, Nanjing 210024, China

[2] College of Oceanography, Hohai University, Nanjing 210098, China

[3] College of Meteorology and Oceanography, National University of Defence Technology, Nanjing 211101, China

break-up by ocean wave should be taken into account in sea ice prediction (Asplin et al. 2014). The ocean wave is the principal energy source for ice break-up in MIZ and plays a dominant role in the process of ice break-up (Kohout and Meylan 2008; Squire et al. 2009). It is also the major factor determining the characteristics and extent of ice fracture (Squire et al. 1995). The ocean waves include both short waves (wind sea) generated locally and surges coming from distant. Surges are generated by distant weather systems and have longer wavelengths (e.g., strong thunderstorms can generate surges with wavelengths exceeding 700 m). Their ranges in frequency and direction are narrower than those generated locally because of the dispersion and dissipation during propagation. And their stochastic characteristics are weakened. The vertical movement of ocean waves results in the fracture of sea ice and the decrease in the size of ice floes. The horizontal movement of the waves forces the ice floes to collide with each other, thus changing their shape and size. Surges can penetrate into the ice cover for a long distance, and sea ice sheets with large area can be broken into floe herd composed of small individual floes under suitable conditions of sea ice and incident wave energy (Squire 2007). Because the ice floe can drift freely and is more sensitive to the drag of the atmosphere and the ocean, vortices made of ice floes can be formed on the sea surface (Dumont et al. 2011). The ice break-up from ocean waves will affect the thermodynamics of sea ice. The fragmentation process of ice floe makes the floe size smaller and the number bigger, which leads to an increase of the total perimeter of ice floes. As a result, the melting of sea ice speeds up in summer because of the enhancement of lateral melting (Steele 1992), and the formation of sea ice is promoted in winter because of the emergence of new ice in the space between the ice floes. Ocean waves affect the formation of sea ice and the exchange of heat flux in polynya and ice margins near shore (Lange et al. 1989), and also change the ocean mixing and air-sea momentum exchange significantly (Janssen 2004; Jenkins 2007).

Numerical sea ice models are powerful tools for scientific research and have been used to tackle many problems, such as, the relationship between sea ice concentration anomalies and temperature anomalies (Armstrong et al. 2003), the influence of atmospheric circulation changes on sea ice transport and formation (Hu et al. 2002), the spatial and temporal variability of ice cover, and the energy exchange on sea ice surface (Makshtas et al. 2003). In these studies, the completeness in the physical process and performance of the sea ice model had an important impact on the research results. It is shown that the absence of wave-sea ice interaction is a likely factor affecting the accuracy of sea ice extent prediction by sea ice model (Holland et al. 2006). The variation of sea ice in MIZ can have a significant impact on the variation of sea ice extent on a global scale (Zhang et al. 2015). Since the target floe size is selective when sea ice is broken up because of waves, the model should be able to characterize the feature of FSD if the effect of sea ice break-up is to be considered in the model. If the floe size distribution is introduced into the sea ice model, the sea ice model will describe the lateral variation of ice floe more accurately, and the model will also be able to describe the climatic effect of sea ice break-up, which will do good for the improvement of sea ice model in climate simulation and climate change prediction.

The theoretical study of sea ice-wave interaction has a long history and rich results have been obtained (Meylan and Squire 1994; Squire et al. 1995; Langhorne et al. 1998; Squire et al. 2009; Williams et al. 2013; just to list a few). However, the application of theoretical fruits to numerical simulation of sea ice climate is still challenging since climate sea ice models cannot depict FSD, let alone the mass transfer of sea ice among floe size categories. In recent years, a few studies on FSD have appeared and promising results have been shown (Zhang et al. 2015; Horvat and Tziperman 2015; Zhang et al. 2016; Roach et al. 2018; Roach et al. 2019). However, there is much work need to be done for further understanding of the parameterization of sea ice break-up because of ocean waves and its impact on climate sea ice modeling.

In this paper, we extended the ice thickness distribution function used in the Community Ice CodE (CICE) version 5.1.2 (Hunke et al. 2015) from the Los Alamos National

Table 1 Experiments of simulation of sea ice on the Southern Ocean

Name of the experiments	Description
EXP_CONTROL	The original version is used with major parameters given in Table 2.
EXP_THERMO	Same as EXP_CONTROL except that the improved lateral melting scheme is used
EXP_IZH15	Same as EXP_THERMO except that sea ice break-up parameterization of IZH15 is added.
EXP_ITH15	Same as EXP_THERMO except that sea ice break-up parameterization of ITH15 is added.

Laboratory to characterize the distribution in both the thickness and the floe size. On this basis, we improved the lateral melting scheme of sea ice and introduced two parameterization schemes of ice break-up because of ocean waves. Through numerical experiments, we performed case studies on parameterization schemes of sea ice fragmentation for ocean waves.

2 Introduction of FSD and handling of associated processes

The FSD, two schemes of sea ice break-up because of ocean waves and an improved scheme for lateral melting of ice floe were introduced into CICE. With the original model variables unchanged, the variables for categories of floe size and associated arrays were added. Except for the basic global variables, the added codes were placed in a new module.

2.1 Introduction of FSD into sea ice model

Like other state-of-the-art sea ice model for climate study, CICE was based on the distribution function of sea ice thickness and the prognostic equation depicting its variation proposed by Thorndike et al. (1975). Following Thorndike et al. (1975), the distribution function of sea ice thickness g was extended to the joint distribution function of sea ice thickness and floe size g_{hs} (the subscript h indicates the sea ice thickness and the subscript s indicates the floe size. Since g was only a function of sea ice thickness in Thorndike et al. (1975), the subscript for the sea ice thickness was omitted). Let g_{hs} keeps the relation $g(h) = \int_0^\infty g_{hs} ds$, so the theory of Thorndike et al. (1975) is inherited. After the introduction of floe size distribution, two additional items (one for the transfer in floe size space and another for the sea ice break-up because of ocean wave) appear in the variation equation of g_{hs} (Eq. (1)) compared with those in Thorndike et al. (1975).

$$\frac{\partial g_{hs}}{\partial t} = -\nabla\cdot\left(\vec{v}\, g_{hs}\right) - \frac{\partial}{\partial h}\left(\dot{h} g_{hs}\right) - \frac{\partial}{\partial s}\left(\dot{s} g_{hs}\right) + \psi_m + \psi_w \quad (1)$$

where 5 items on the right-hand side are variation rate for advection, transportation in thickness space, transportation in floe size space, mechanical deformation, and ice break-up, respectively.

In the implementation of introducing FSD into CICE, the 5 categories of floe size defined by the World Meteorological Organization (WMO) (WMO 2014) were subdivided into 11 categories and a category of minute size (0–20 m) was added (Details were shown in Table 2 of part 3). With the equation

$$\int_h^{h+dh}\int_s^{s+ds} g_{hs}(h,s)\, ds\, dh = A_{hs} \quad (2)$$

sea ice concentration in thickness category h-h + dh and floe size category s-s + ds (A_{hs}in Eq. ((2)) can be computed.

2.2 Improvement on the calculation of lateral melt of sea ice

Since there was no information on the distribution of floe size in CICE, the model calculated the lateral melting rate of sea ice with an assumed constant floe size (300 m in diameter), and the effects of individual floe size were not taken into account. With the introduced the information of FSD, the enhancement mechanism of lateral melting caused by the sea ice break-up can be described.

Following Steel (1992), the lateral melting rate (the sea ice concentration melted per unit time) of ice floe with size S (denoted by diameter) is

$$M_D = m_1 \Delta T^{m_2} \pi / (\alpha S) \quad (3)$$

where m_1, m_2, and α are constants (see Table 2), ΔT is the difference between sea surface temperature and ice bottom surface temperature.

Table 2 Major specific parameters used in the work

Parameter	Description
Floe size category	12, the middle values are 10 m, 33 m, 60 m, 87 m, 167 m, 300 m, 433 m, 875 m, 1625 m, 4000 m, 8000 m, and 20000 m
Constants in Eq. (3)	m_1 = 1.6E-6 m/s/K^(-m_2), m_2 = 1.36 and α = 0.66
C_c in Eq. (6)	9.0E-5
C_b in Eq. (6)	A unitless value ranging from 0.1 to 0.5
$S_{\min}$ and S_{max} in Eq. (7)	$S_{\min}$=10 m and S_{max} = 20000 m
c_g and D in Eq. (8)	c_g = 4.5 m/s and D = 1.5 E5 m
R in Eq. (8)	R is computed on 10 m grids for each thickness type and then interpolated in space of floe size

With Eq. (3), the lateral melt rate of sea ice for each floe size, which gives a contribution to the transportation in floe size space (regarding the melt rate as the velocity in floe size space, the third item on the right-hand side of Eq. (1) is the transportation in flux form), is calculated. Then the area fraction of each floe size after lateral melt is obtained. By summing the results over the floe size categories, the predicted sea ice concentration after lateral melt for a certain thickness category is got.

2.3 Introduction of parameterization for sea ice break-up

Considering only the sea ice changes caused by ocean waves, the evolution equation of the joint distribution function of sea ice thickness and floe size can be expressed as follows:

$$\frac{\partial g_{hs}}{\partial t} = \psi_w \tag{4}$$

$$\psi_w = -Q(h,s)g_{hs}(h,s) + \int_0^{\infty}\beta\left(s^{'},s\right)Q\left(h,s^{'}\right)g_{hs}\left(h,s^{'}\right)ds^{'} \tag{5}$$

where Q is a redistribution function of probability, which determines whether the sea ice breakup will happen and what category of floe ice will get involved; β is a transfer function of floe size, which indicates how one category of floe size can be transformed into another by the process of ice break-up; h is the ice thickness; s and $s^{'}$ are the sizes of target and source ice floe (involving transformation from source category of floe size (s') to target (size s) due to sea ice fragmentation) respectively.

2.3.1 Implementation of Zhang et al. (2015) (IZH15)

Following Eq. (15) in Zhang et al. (2015), Q in Eq. (5) is expressed as follows:

$$Q(h,s) = max\left[\int_h^{h+dh}\int_0^{\infty}g_{hs}\left(h^{'},s^{'}\right)ds^{'}dh^{'} - \int_h^{h+dh}\int_s^{\infty}g_{hs}\left(h^{'},s^{'}\right)ds^{'}dh^{'}/C_b, 0\right]C_c \tag{6}$$

where the expression Q has been extended into the ice thickness space and s is used instead of l; An additional constant coefficient C_c (see Table 2) is introduced and C_b is no longer a constant but varies with ice thickness (the thicker the ice, the smaller the C_b); h and $h^{'}$ are the ice thickness and s and $s^{'}$ are the size of ice floe.

The formula of the transfer function of floe size β in Eq. (5) follows Eq. (14) in Zhang et al. (2015) with l_2 replaced by s and $S_{\min}$ by $s^{'}$:

$$\beta\left(s^{'},s\right) = \begin{cases} \frac{1}{C_2s^{'}-C_1s^{'}} & C_1s^{'} \le s \le C_2s^{'} \\ 0 & s < C_1s^{'} \text{ or } s > C_2s^{'} \end{cases} \quad C_1 = (s_{\min}/s_{\max})^2, C_2 = 1-C_1 \tag{7}$$

where $S_{\min}$ and S_{max} are the minimum and maximum floe size in the floe size categories, respectively (see Table 2).

2.3.2 Implementation of Horvat and Tziperman (2015) (IHT15)

Following Eq. (22) in Horvat and Tziperman (2015), Q is expressed as follows with r replaced by s:

$$Q(h,s) = \frac{c_g}{D}\left(\int_0^{s} s^{'}R\left(h,s^{'}\right)ds^{'}/D\right) \tag{8}$$

where c_g is the group speed of ocean wave, D is the grid size of the model, and R is the normalized number of fractures deduced from a sea surface height model (Horvat and Tziperman 2015) (see Table 2).

Following Eq. (21) in Horvat and Tziperman (2015), the formula of the transfer function of floe size is expressed as follows with s replaced by $s^{'}$ and r by$s$:

$$\beta\left(s^{'},s\right) = \begin{cases} \frac{s^{'}R(s,h)}{\int_0^{s^{'}} sR(s,h)ds} & s < s^{'} \\ 0 & s > s^{'} \end{cases} \tag{9}$$

In the parameterization for sea ice break-up from Horvat and Tziperman (2015), the spectrum of ocean waves plays a vital role in determining the distribution of floe size.

3 Design of numerical experiments

Two groups (denoted by G1 and G2) of experiments had been designed. In the experiments, the Bretschneider wave spectrum, in which the mean zero-crossing period is 6 s and significant wave height is 2 m, was used. The spectrum is divided into 8 parts with periods of wave components ranging from 4 to 18 s. The midvalues of floe size for the 12 floe size categories are shown in Table 2.

3.1 G1: Experiments of sea ice break-up for a single grid

To explore the behavior of floe size redistribution and FSD feature for swell fracture in the two different ice fragmentation schemes, an idealized scenario of ice fragmentation was proposed. In the presumed initial conditions, the area fraction for the category with the biggest floe size of each thickness type is 0.2, while that for other floe size category is 0. Assuming that ocean wave with the given spectrum is always available, the

model is integrated for 100 steps with only the process of sea ice break-up for ocean wave considered. Major specific parameters used in the work are shown in Table 2.

3.2 G2: Experiments of simulation of sea ice on the Southern Ocean

To test whether the introduced FSD and implementing ice fragmentation schemes can create features of ice floes often observed in the MIZ, four numerical experiments for sea ice on the Southern Ocean as described in Table 1 were designed. In all experiments, the CICE was integrated for 20 years. In the simulations, the mixed layer ocean module included in CICE was used to depict the thermal variation of ocean surface temperature. The model was configured with a displaced pole global orthogonal grid (the coarse grids situate at midlatitudes with the maximum area of about 7.5 104 km^2 and the finer grids at the polar region with the minimum area of about 1.5 104 km^2). Atmospheric forcing, such as wind, air temperature, and specific humidity 4 times a day, were from the Coordinated Ocean-ice Reference Experiments—Phase II (CORE-II) datasets (Large and Yeager 2009); Monthly mean precipitation rate and cloud cover fraction were from CORE-II and the International Satellite Cloud Climatology Project (ISCCP) (Stubenrauch et al. 2013) respectively; Longwave fluxes were computed based on Rosati and Miyakoda (1988); Following the Arctic Ocean Model Inter-comparison Project (AOMIP) shortwave forcing standard, downward short wave fluxes were calculated using solar declination angle and then reduced using a function of cloud fraction. Sea ice concentration from the Hadley Centre Sea Ice and Sea Surface Temperature data set (HadISST) was used to evaluate the deficiency in the modeled distribution of sea ice concentration. Monthly means were got by averaging sea ice concentration from 1988 to 2009.

In the control run (EXP_CONTROL), the original CICE5.1.2 was used with major parameters given in Table 3 in the Appendix; In EXP_THERMO, FSD was predicted, and the improved lateral melting scheme was used, whereas the ice fragmentation was not considered; In EXP_IZH15 and EXP_ITH15, ice floe break-up parameterization schemes of IZH15 and ITH15 were switched on respectively besides using configuration in EXP_THERMO (see Table 1). Parameters such as the number of floe size categories and those used in the break-up schemes are given in Table 2.

Initial values of the area fraction of all floe size categories were derived from sea ice concentration with formula proposed for observed sea ice by Perovich and Jones (2014).

Since the mixed layer ocean uses constant mixed layer depth and submixed layer heat flux, the influence of deep ocean is not transient. The adjustment of sea temperature as well as sea ice towards equilibrium is quick. There is no discernable long-term trend other than annual variation in the simulated sea ice concentration averaged over the ocean south of 45° S in all experiments (Fig. 8 in the Appendix). A 20-year integration is enough for each experiment.

4 Results

Results from G1 and G2 designed in part 3 are shown in 4.1 and 4.2 respectively.

4.1 Results from G1

From the result of simulations in G1, it is clear that after fragmentation begins, the sea ice area fraction of the biggest floe size category decreases and the sea ice area experiences redistribution with a shift towards categories of smaller floe size (Fig. 1). There are differences in the characteristics of the sea ice area shift between IZH15 and IHT15. In IZH15, the area transfer is continuous; during the process of sea ice break-up, area fraction of the category with the second largest floe size increases first and decrease later; this process continually propagates towards a category with smaller floe size; for the thick ice, due to the decreased efficiency of sea ice crushing, the speed of sea ice area variation mentioned above slows down (Fig. 1 a and c). In IHT15, the possibility of a floe break-up is dependent on the wavelength, so the target size of ice floe to be broken up into is determined by ocean waves; the dominant target size of ice floe fragmentation of ice thickness type 1 is about 170 m, while that for the thickness type 5 is about 90 m; similarly, for the thick sea ice, the speed of area fraction variation is slowed down because of the decrease of ice break-up efficiency (Fig. 1 b and d). Compared with the case of thin ice, the extent of the floe size after fragmentation in thick ice is narrower. In the study, wave damping is not accounted for, therefore the wave climate remains very energetic deep in the ice pack where the ice is thicker compared with the ice edge. In reality, ice fragmentation due to ocean wave for thick ice cannot be such strong as the case in (c) and (d).

4.2 Results from G2

Results for the impact of modification in the lateral melting calculation and parameterization of sea ice break-up are shown in this part.

4.2.1 Results from improved lateral melting scheme without sea ice break-up

After introducing the FSD into CICE, the accuracy of calculation of the lateral melting rate is improved. Compared with results from EXP_CONTROL, the simulated sea ice

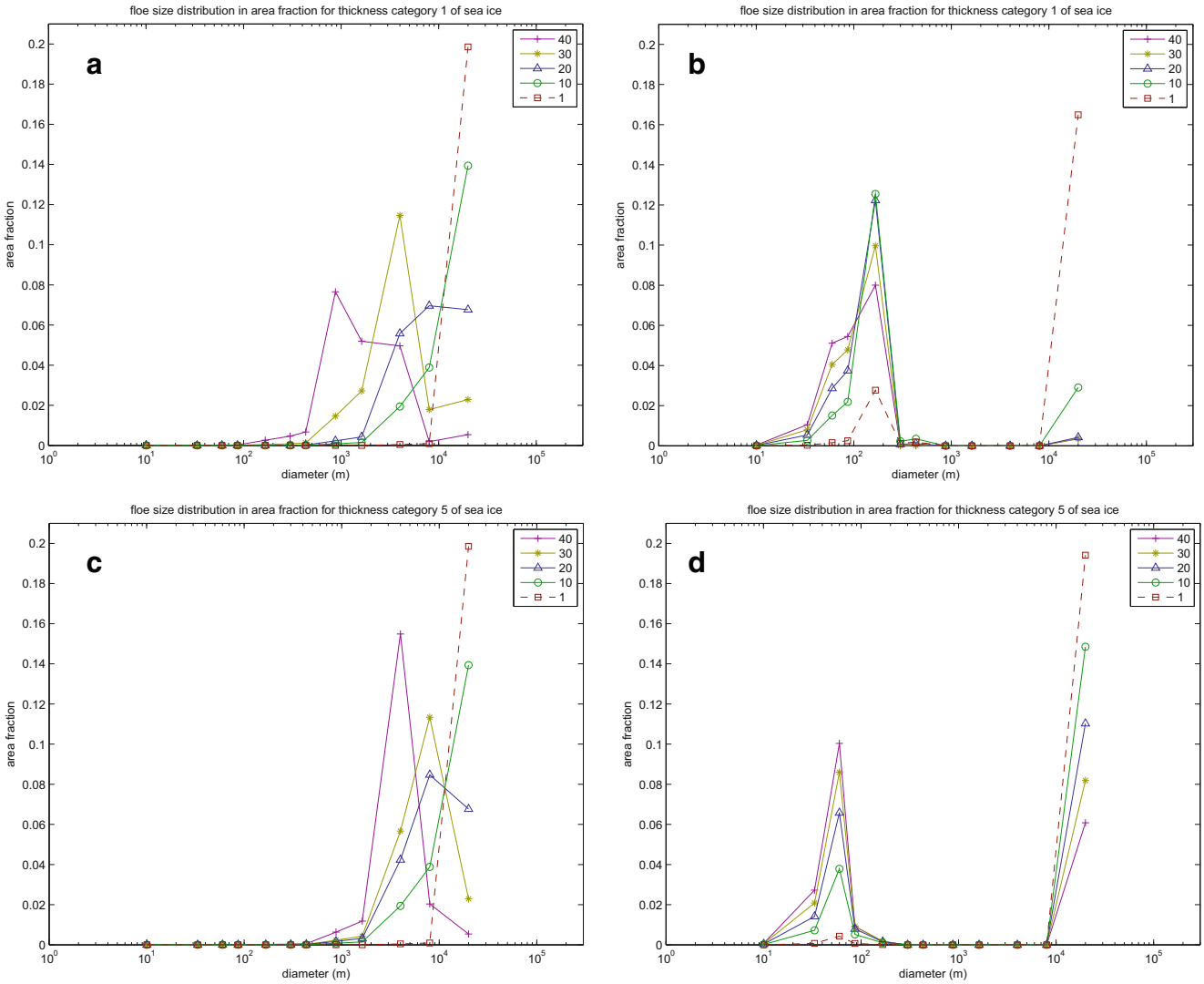

Fig. 1 Distribution of sea ice area fraction with floe size (diameter) simulated with **a**, **c** IZH15 and **b**, **d** IHT15 for **a**, **b** the thickness categories 1 and **c**, **d** 5. The numbers in the box of legend denote times of ice break-up. The units for sea ice area fraction and floe size are × 100% and *m* respectively. The thickness type 1 is 0–0.64 m and the thickness type 5 is 4.57–9.33 m

concentration from EXP_THERMO is reduced (Fig. 2). In March, the differences are mostly discerned at the outer edge of the ice pack in the Weddell Sea and the Ross Sea, which are only partially covered by dispersing ice floes. The biggest difference is about 6%. In September, the magnitude of the difference is much smaller with a maximum value of 0.4% (compare Fig. 2d with Fig. 2b). The outer edge of the simulated ice pack is more circular compared with that of observation due to the absence of the influence by ocean currents in the model (compare Fig. 2c with Fig. 3b). The areas of reduced sea ice concentration induced by improvement in lateral melting calculation align along a geometrical circle which is on the edge of sea ice extent (Fig. 2d). With introducing FSD, the improved lateral melting scheme helps to reduce the surplus sea ice in the simulation results (see Fig. 2 and Fig. 3). It is clear that with the mechanism of sea ice break-up due to ocean surface waves not considered, the impact of prognostic FSD on sea ice concentration simulation is not significant. The lateral melts rate is smaller for sea ice in the floe size category with larger floe size, whereas the patterns of lateral melt rate distribution of sea ice in different floe size categories are similar for the same month (see Fig. 9 in the Appendix).

4.2.2 Results from simulations with sea ice break-up and improved lateral melting scheme

Due to the rough slab ocean, the simulated sea ice extent over the Southern Ocean, especially in September, from

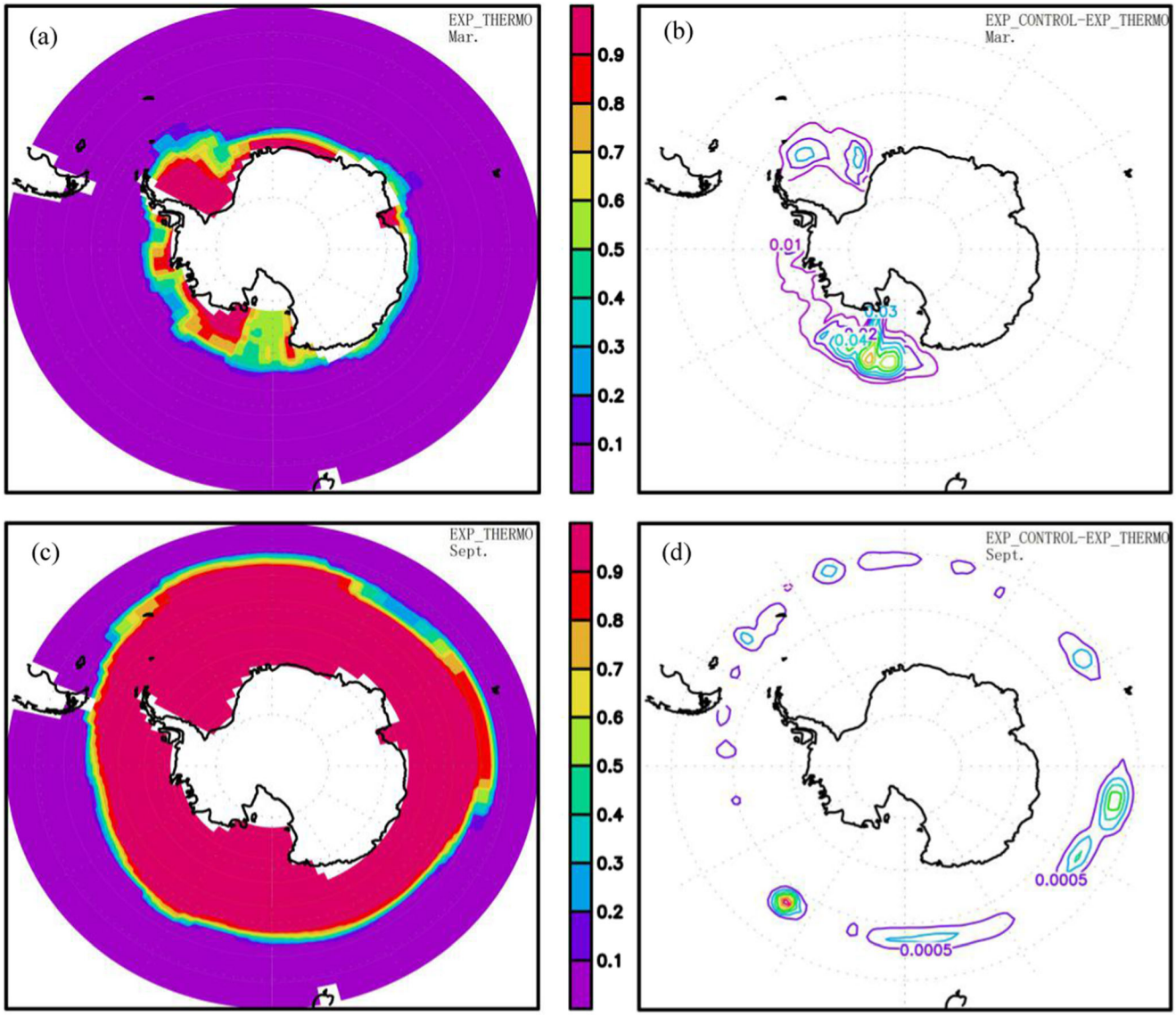

Fig. 2 Simulated sea ice concentration in **a**, **c** EXP_THERMO and its deviation **b**, **d** from that in EXP_CONTROL (EXP_CONTROL minus EXP_THERMO) for **a**, **b** March and **c**, **d** September. The unit is × 100% and the contour intervals in **b** and **d** are 0.01 × 100% and 0.0005 × 100% respectively

EXP_CONTROL is larger than that from observation (compare Fig.4e with Fig.3a and Fig. 4f with Fig. 3b). After introducing the mechanism of sea ice break-up, the surplus sea ice cover in March is reduced significantly, whereas there is no obvious difference in the simulated sea ice concentration in September among the experiments in G2 (Fig. 4). To discern the effect of swell fracture on sea ice freezing, making analysis in a shorter time scale may be better. The patterns of reduced sea ice concentration are similar from EXP_ IZH15 and EXP_ IHT15. This is because there are more possibilities in sea ice break-up of thinner ice in both schemes. The overall lateral melts of sea ice in March on the Weddell Sea from EXP_ IZH15 is stronger than that from EXP_ IHT15 (compare Fig. 4a with Fig. 4c). This is because the amount of sea ice with smaller floe size is larger from EXP_ IZH15 (compare Fig. 5a with Fig. 5b), which favors stronger lateral melt.

There are significant differences in patterns of area fraction distribution from EXP_ IZH15 and EXP_ IHT15 (Fig. 5). For the floe size category 1 (diameter is roughly 10 m), the simulated sea ice area fraction is larger from EXP_ IZH15 (compare Fig. 5a with Fig. 5b and Fig. 5e with Fig. 5f). This is because IZH15 is more efficient in transferring sea ice mass from larger ice floes to the ice floes of floe size category 1. The area fraction for the floe size category 12 (diameter is roughly 20 km) is small from both schemes due to ice break-up and mass transfer towards smaller ice floes. Contrary to the situation for the floe size category 1, the simulated sea ice area fraction is

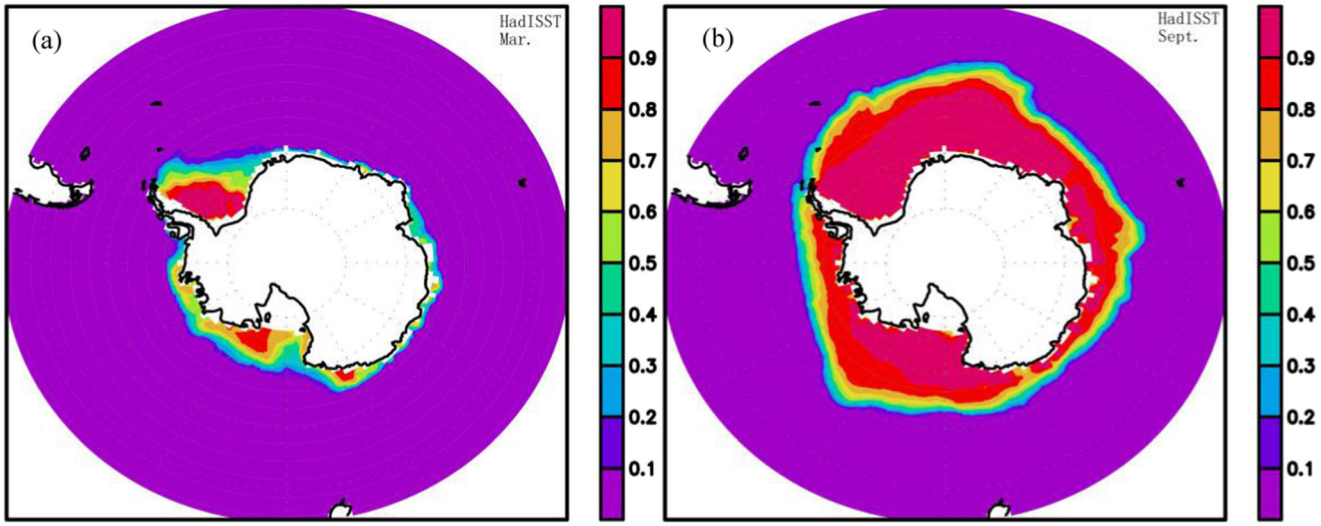

Fig. 3 The sea ice concentration for **a** March and **b** September from HadISST. The unit is × 100%

larger from EXP_IHT15, especially in September, for the floe size category 12 (compare Fig. 5d with 5c and Fig. 5h with 5g). This is because IHT15 is selective in transferring sea ice mass from the large ice floes to smaller ones since its action in breaking up the ice depends on the wavelength of the ocean waves.

There are complicated interactions between ocean and sea ice even though a simple ocean component is used here. With effects of sea ice fragmentation, the lateral melt of sea ice increases and the sea ice concentration decreases. Although the decreased sea ice concentration allows more absorption of solar radiation in the water, the ocean temperature does not increase significantly due to the loss of latent heat for melting the sea ice in the region of significant sea ice reduction (R1 and R2 in Fig. 6). However, the change of floe mass due to swell fracture influences the pattern of ice stream, which in turn redistributes the sea ice mass over the ocean. Accompanying the divergence of sea ice, the locally reduced sea ice decreases sea ice melt as well as assumption of latent heat from the ocean, contributing to the increase of sea surface temperature there (B1 and B2 in Fig. 6).

In summer, the ice floe melts both laterally and vertically. In regions with significant decrease of sea ice concentration, there are also significant decrease in ice thickness (regions D in Fig. 7). This reflects the thermodynamics controlling the evolution of sea ice. The variations of sea ice are also influenced by sea ice dynamics. The fragmentation of ice floes can change the inner force due to collision between floes, which had been represented through parameterization in CICE. The change of inner force leads to variation of sea ice velocity. Sea ice convergence anomalies as shown in Fig. 6 can bring about ridging, which increases the thickness of sea ice in regions A in Fig. 7.

5 Summary and discussions

The implementing prognostic FSD in CICE has been fulfilled and the calculation of lateral melting of sea ice has been improved by taking advantage of the additional information of floe size. Two schemes of swell fracture have also been introduced. Experiments were designed to examine the differences of sea ice area transfer among categories of floe size between the two introduced swell fracture schemes, the influences of improved lateral melting on sea ice simulation without sea ice break-up, and the overall effects of sea ice break-up and improved lateral melting on sea ice modeling. IZH15 deals with the sea ice fragmentation due to lateral collision and vertical movement induced by an ocean wave with no explicit constraint of ocean wave features on the mass transfer of floes towards smaller ones, whereas ITH15 focuses on the sea ice break-up due to bending failure induced by vertical movement of ocean wave. The transfer of sea ice area among categories of floe size is continuous in IZH2015 and selective in IHT2015. If the mechanism of sea ice break-up due to ocean surface wave is not considered, the effect of FSD on sea ice simulation is small. This is because the positive feedback loop as mentioned by Asplinet al. (2014) is cut off. Under the combined effect of improved lateral melt and sea ice break-up, the surplus sea ice cover is reduced greatly on the Ross Sea and the Weddell Sea in March. The sea ice fragmentation in September does not make a significant difference in the distribution features of simulated sea ice concentration. The patterns of reduced sea ice concentration are similar in EXP_ IZH15 and EXP_IHT15. The simulated area fraction for the individual floe size category is different due to the difference in transferring sea ice mass between the two ice break-up schemes.

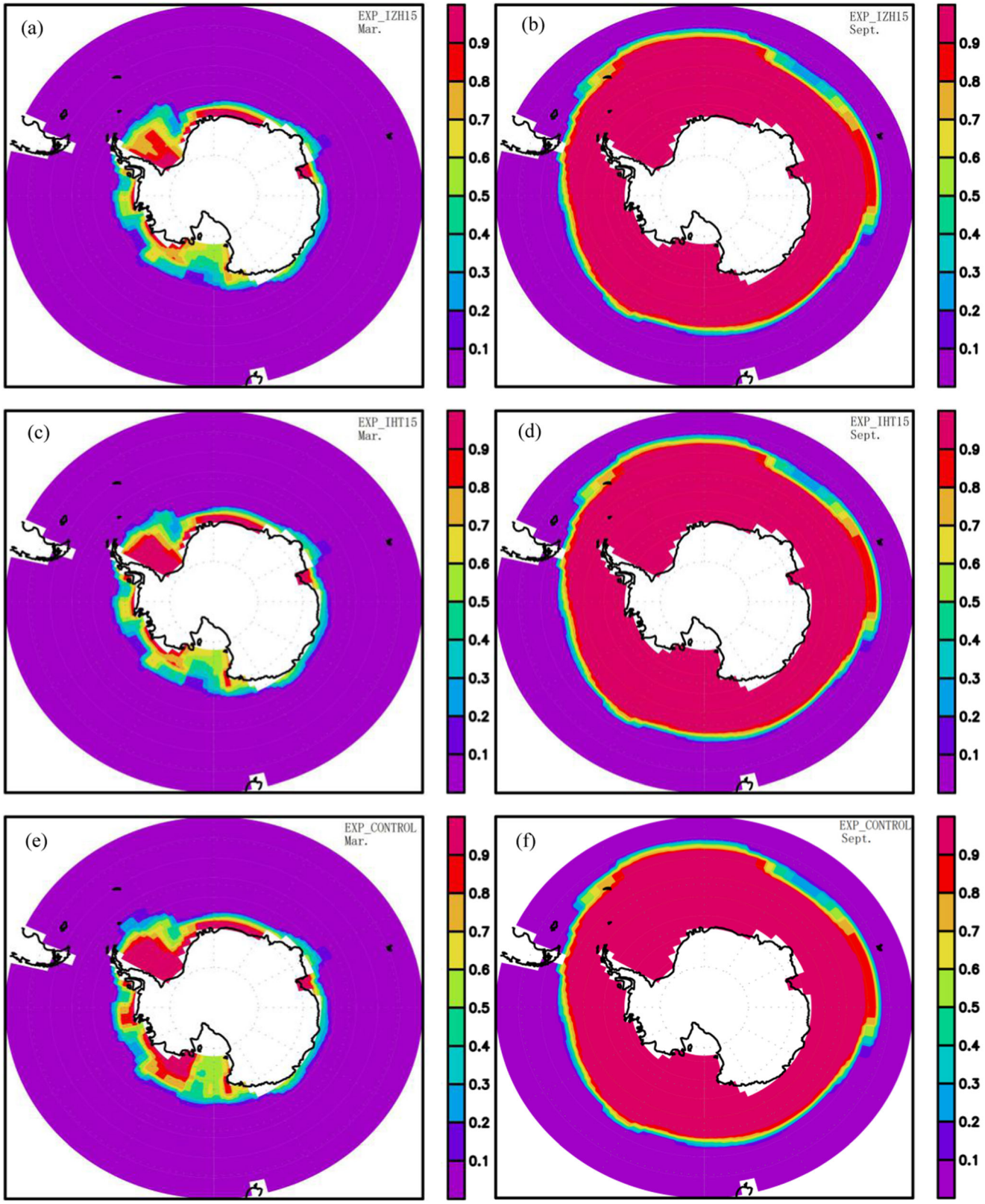

Fig. 4 Simulated sea ice concentration in **a**, **b** EXP_IZH15, **c**, **d** EXP_IHT15, and **e**, **f** EXP_CONTROL for **a**, **c**, **e** March and **b**, **d**, **f** September. The unit is × 100%

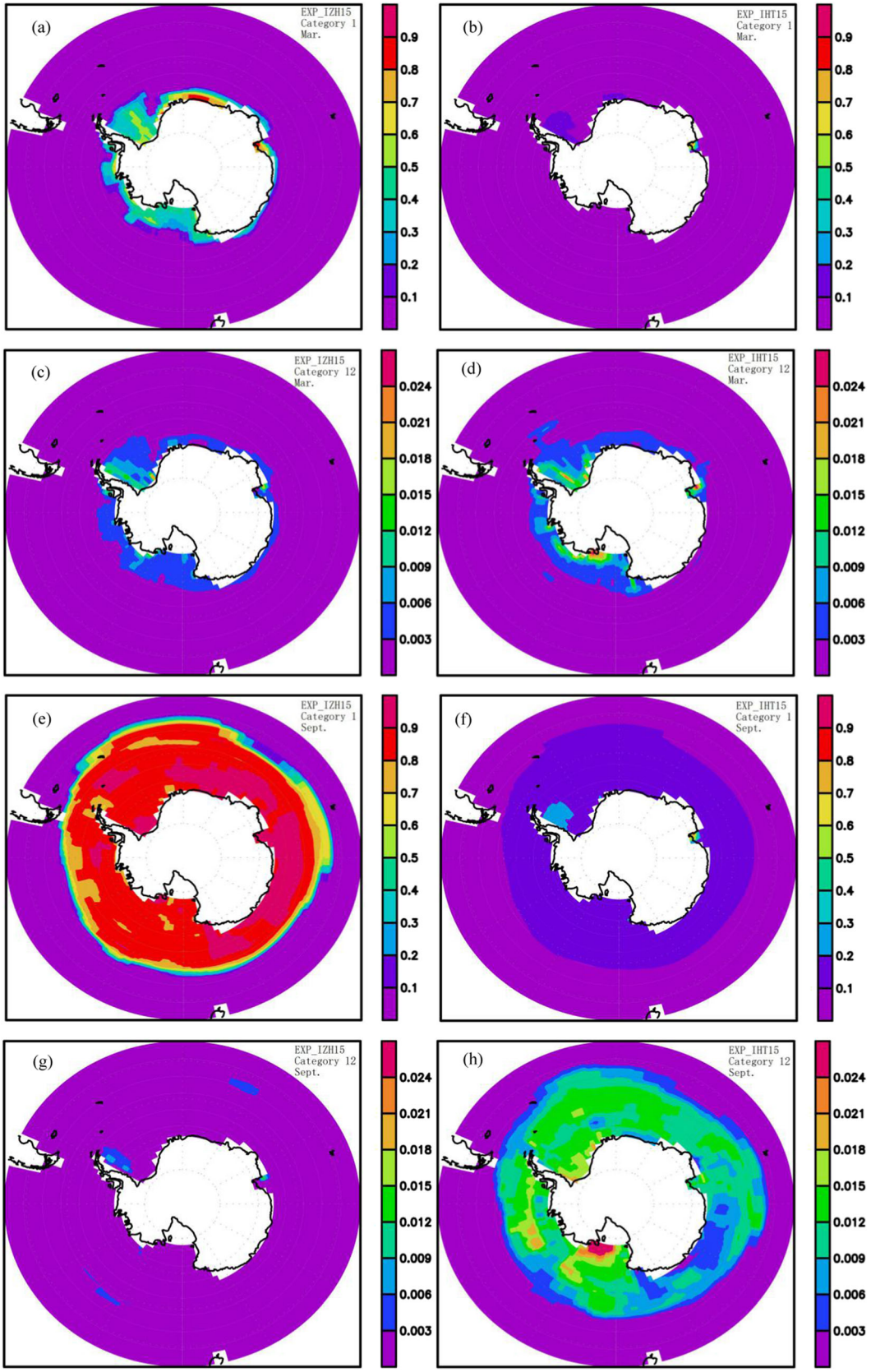

Fig. 5 Simulated sea ice area fraction of **a**, **b**, **e**, **f** floe size categories 1 and **c**, **d**, **g**, **h** 12 in **a**, **c**, **e**, **g** EXP_IZH15 and **b**, **d**, **f**, **h** EXP_IHT15 for **a**–**d** March and **e**–**h** September. The unit is × 100%

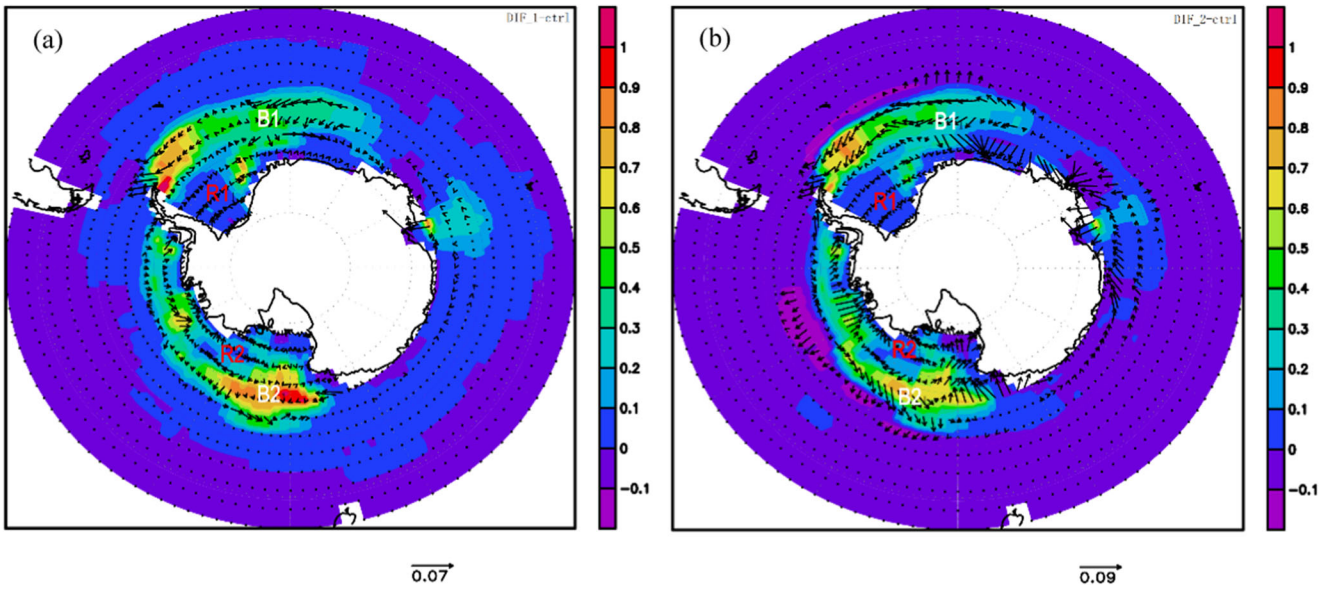

Fig. 6 Difference of sea surface temperature and sea ice current in March **a** between EXP_IZH15 and EXP_CONTROL and **b** between EXP_IZH15 and EXP_CONTROL. The units for sea surface temperature and sea ice current are °C and m/s respectively. R1 and R2 denote regions with sea ice reduction and B1 and B2 denote regions with sea ice divergence

In the National Center for Atmospheric Research (NCAR) version of CICE (https://github.com/ESCOMP/CESM_CICE5), floe size is parametrized as a function of the ice concentration given by Lüpkes et al. (2012), and the form drag associated with floe edges has been computed (Tsamados et al. 2014). In the work, floe size is prognostic whereas the influence of floe edges on the surface momentum exchange at the ice-atmosphere interface has not been considered.

In the simulations, the Bretschneider wave spectrum is used, and the damping of the ocean waves due to sea ice is not considered. To better simulate the effect of swell fracture on sea ice, ocean waves from the state-of-the-art ocean wave model, which are more reasonable, should be used. Recently, experiments which are the first to include two-way interactions between prognostically evolving waves and sea ice on a global domain have been presented (Roach et al. 2019). Under such framework, the impact of varying wave climate on sea ice fracture can be studied better. In the experiments, the parameter D in Eq. (8) is fixed, whereas grid size is variable in the model. This simplification will also have influences on the modeling results.

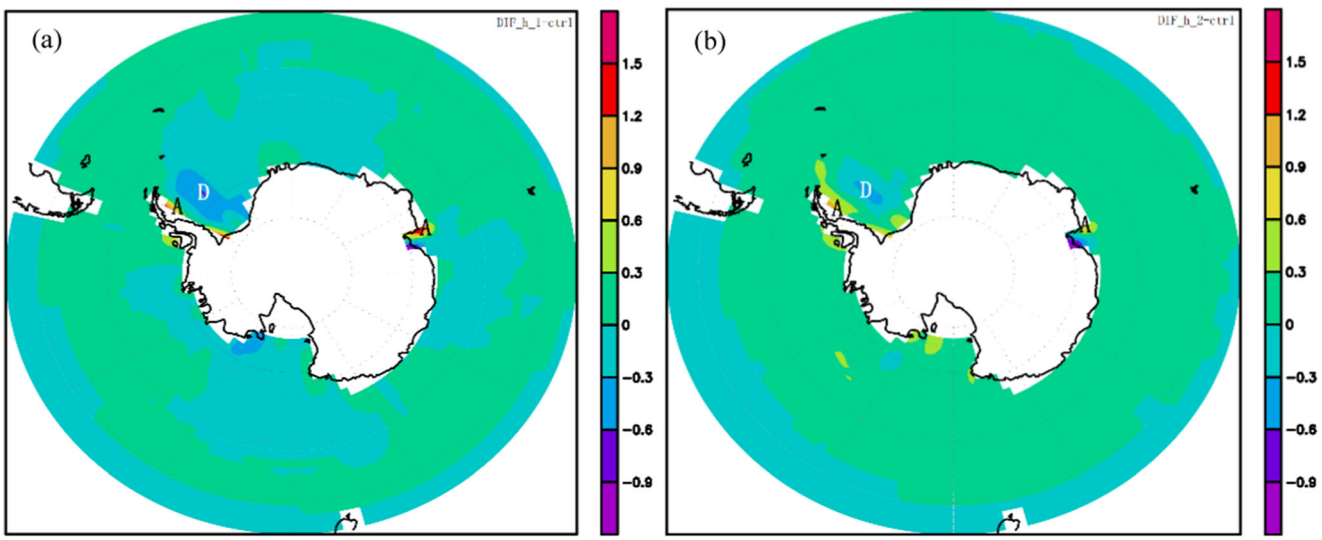

Fig. 7 Difference of sea ice thickness in March **a** between EXP_IZH15 and EXP_CONTROL and **b** between EXP_IZH15 and EXP_CONTROL. The unit for sea ice thickness is m. D denotes regions with sea ice thickness decrease and A denotes regions with sea ice thickness increase

The spatial and temporal variability of floe size is very important for such studies as ocean wave refraction. Since FSD representing the nature of the sea ice is rarely available to the user, the sea ice model with prognostic FSD is an important tool to study the features of this parameter. It is shown from this study that parameterization schemes of sea ice fragmentation due to ocean waves have substantial influence on the modeling of the distribution of sea ice area fraction with different floe size. The study of the impact of parameterization schemes of sea ice fragmentation on sea ice modeling needs more work.

Since lateral melts does not affect the total number of floes, the cumulative number of floes should be conservative. Basing on that, an additional item, i.e., $s\overset{\cdot}{}_{s}^{2} g_{hs}$ should be added on the right-hand side of Eq. (1) according to Horvat and Tziperman (2015) and Roach et al. (2018). The effect of $s\overset{\cdot}{}_{s}^{2} g_{hs}$ on the variation of FSD also deserves further study.

Acknowledgments The cloud amount data (CA_ISCCP_D1_AMPM_19842007.nc) was downloaded from the Climserv Data Center of IPSL/CNRS. Most of the work was planned and carried out during Liu's visits to Cecilia M. Bitz at the University of Washington in Seattle.

Funding This study was partly supported by the National Key Research and Development Program of China (Grant No. 2017YFA0604104) and the Fundamental Research Funds for the Central Universities in China (Grant No. 2019B00214).

Appendix

Table 3 Major parameters used in EXP_CONTROL

Parameter	Adoption
Type of ice thickness distribution conversions	Linear function
Thermodynamics scheme	Mushy
Thermal conductivity in interior ice layers	Bubbly brine
Mushy layer gravity drainage physics	Channel radius for rapid mode drainage is 0.5 10^{-3} m; critical Rayleigh number for rapid mode drainage is 10; aspect ratio for rapid mode drainage is 1; slow mode drainage strength is − 5.0 10^{-8} m/s/K; critical liquid fraction porosity cutoff for slow mode drainage is 0.05; liquid fraction of congelation ice is 0.85.
Sea ice rheology	Elastic–Viscous–Plastic (EVP) sea ice rheology
Advection algorithm	Incremental remapping transport scheme
Formulation of sea ice strength	Rothrock75
Participation scheme for mechanical redistribution	Exponential dependence on sum of areas in categories 0 to n.
Redistribution function for ridging	Exponential function
Parameter determining e-folding scale of ridged ice	3 ($m^{1/2}$)
Ratio of ridging work to potential energy change in ridging	17
Scheme to calculate surface albedos and internal fluxes of short wave	Delta-Eddington
Albedos for ice and snow thicker than 0.3 m	Albedos of visible and near-infrared bands are 0.78 and 0.36 respectively for ice; albedos of visible and near-infrared bands are 0.98 and 0.70 respectively for snow.
Critical pond lid thickness for topo ponds	0.01 m
Snow depth for transition to bare sea/pond ice	0/0.03 m
Alter e-folding time scale for flushing	0.001
Melt pond refreezing parameterization	Stefan approximation
Minimum/maximum retained fraction of meltwater	0.15/1
Ratio of pond depth to pond area fraction	0.8 m

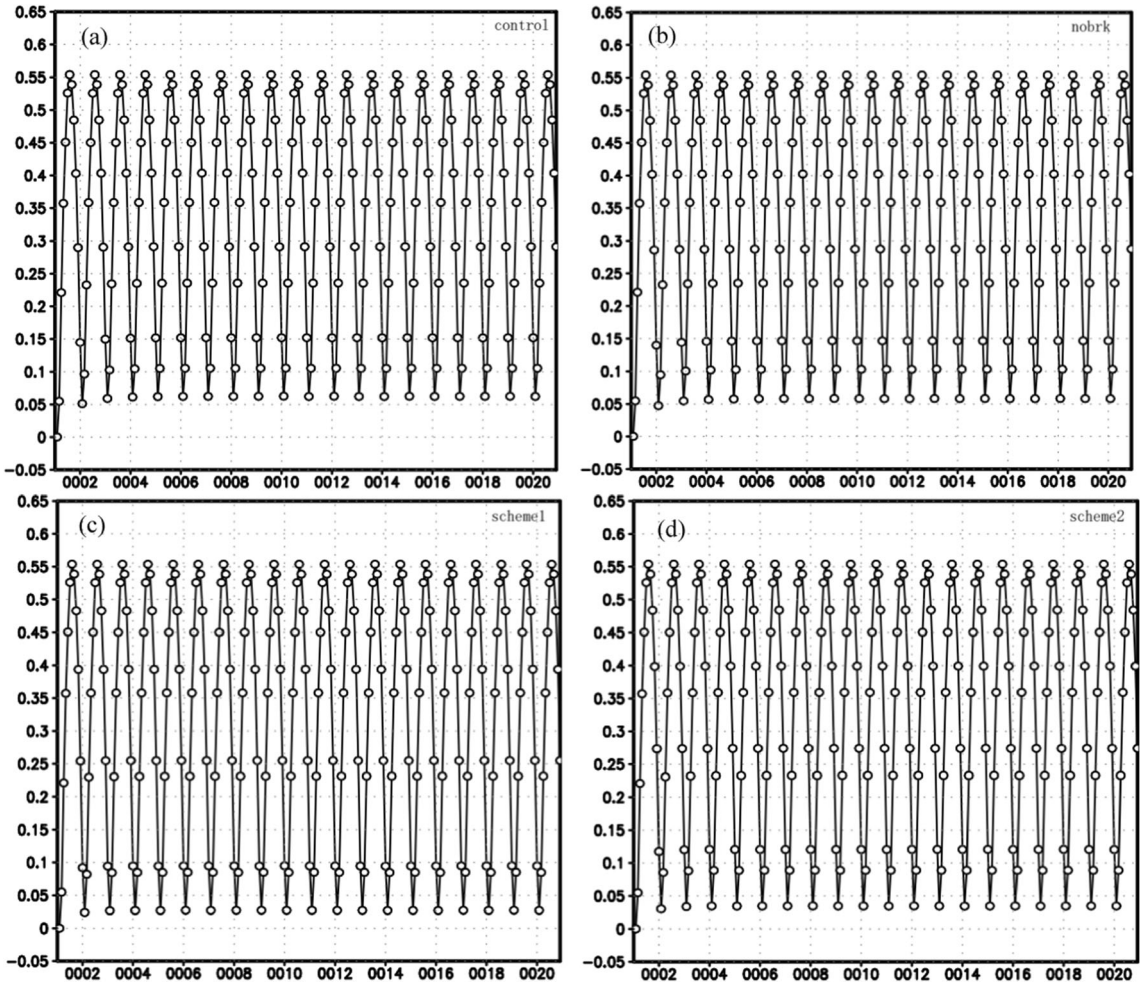

Fig. 8 Evolution of sea ice concentration averaged over the ocean south of 45 °S from (a) EXP_CONTROL, (b) EXP_THERMO, (c) EXP_IZH15 and (d) EXP_ITH15. The horizontal axis is time (year) and the vertical axis is sea ice concentration (the unit is × 100%)

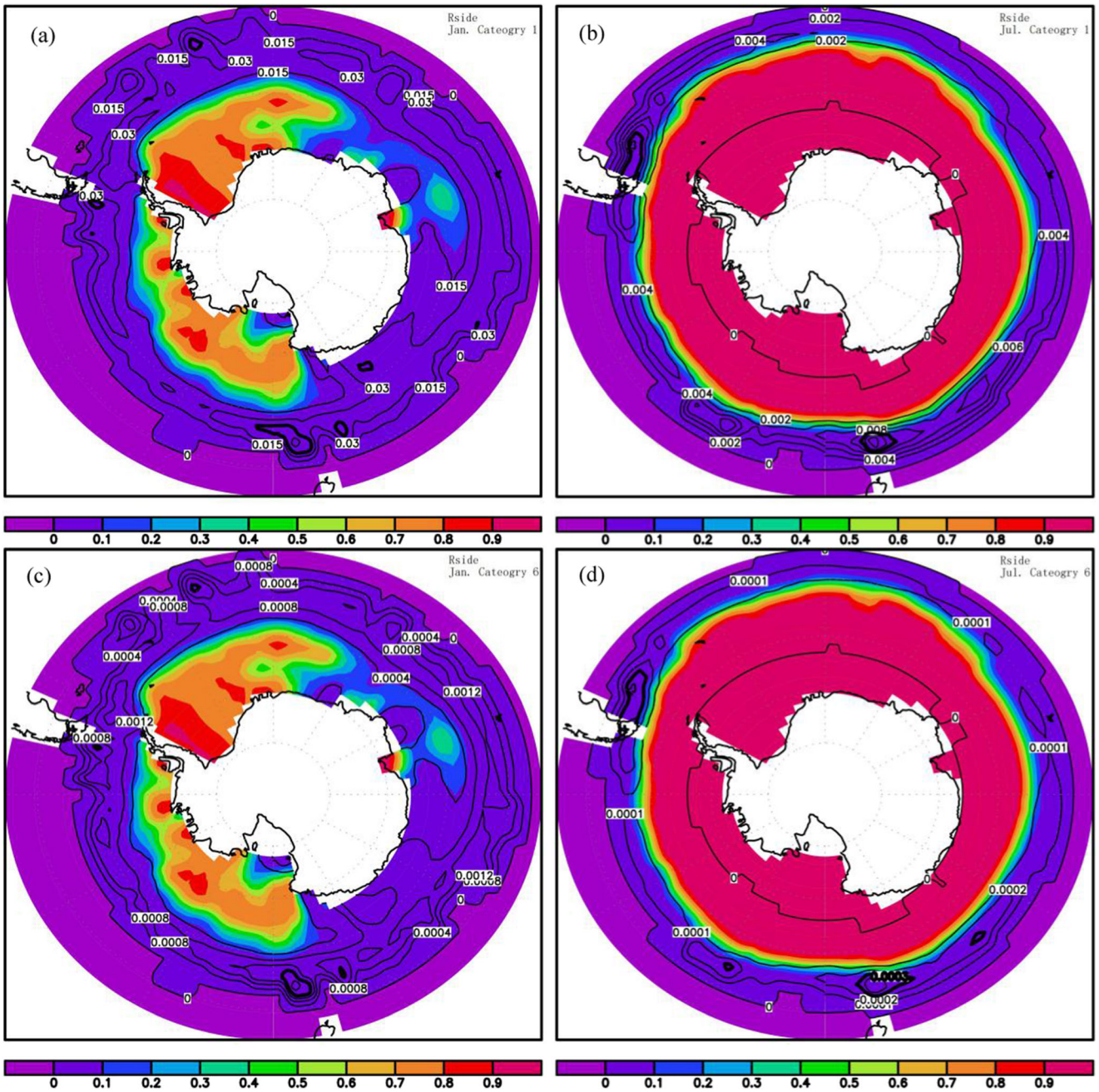

Fig. 9 Fraction of ice that melts laterally (black lines) in one time step (3600 s) with no consideration of wave breaks in (a,c) January and (b,d) July for (a,b) floe size category 1 and (c,d) 6. The simulated sea ice concentration is also shown in shaded contours. The contour interval for (a) is 0.015 with lines of contour level 0.045 thickened; the contour interval for (b) is 0.002 with lines of contour level 0.01 thickened; the contour interval for (c) is 0.0004 with lines of contour level 0.0016 thickened; the contour interval for (d) is 0.0001 with lines of contour level 0.0003 thickened

References

Armstrong AE, Tremblay LB, Mysak LA (2003) A data-model intercomparison study of Arctic sea-ice variability. Clim Dyn 20:465–476

Asplin MG, Scharien R, Else B, Howell S, Barber DG, Papakyriakou T, Prinsenberg S (2014) Implications of fractured Arctic perennial ice cover on thermodynamic and dynamic sea ice processes. J Geophys Res Oceans 119:2327–2343

Dumont D, Kohout A, Bertino L (2011) A wave-based model for the marginal ice zone including a floe breaking parameterization. J Geophys Res 116:C04001

Holland MM, Bitz CM, Tremblay B (2006) Future abrupt reductions in summer Arctic sea ice. Geophys Res Lett 33:L23503

Horvat C, Tziperman E (2015) A prognostic model of the sea ice floe size and thickness distribution. Cryosphere 9:2119–2134

Hu A, Rooth C, Bleck R, Deser C (2002) NAO influence on sea ice extent in the Eurasian coastal region. Geophys Res Lett 29:2053

Hunke EC, Lipscomb WH, Turner AK, Jeffery N, Elliott S (2015) CICE: The Los Alamos Sea ice model documentation and software user's manual version 5.1. Tech. Rep.LA-CC-06–012. http://www.ccpo.odu.edu/~klinck/Reprints/PDF/cicedoc2015.pdf. Accessed 26 August 2019

Janssen P (2004) The interactions of ocean waves and wind. Cambridge Univ Press, Cambridge

Jenkins AD (2007) The interaction of ocean surface processes, waves, and turbulence in the adjacent boundary layers. In: Garbe CS et al (eds) Transport at the air-sea interface: measurements, models and parameterizations. Springer, Berlin, pp 145–158

Kohout AL, Meylan MH (2008) An elastic plate model for wave attenuation and ice floe breaking in the marginal ice zone. J Geophys Res 113:C09016

Lang A, Yang S, Kaas E (2017) Sea ice thickness and recent warming. Geophys Res Lett 44:409–418

Lange MA, Ackley SF, Wadhams P (1989) Development of sea ice in the Weddell Sea. Ann Glaciol 112:92–96

Langhorne PJ, Squire VA, Fox C, Haskell TG (1998) Break-up of sea ice by ocean waves. Ann Glaciol 27:438–442

Large WG, Yeager SG (2009) The global climatology of an interannually varying air-sea flux data set. Clim Dyn 33:341–364

Laxon S, Peacock N, Smith D (2003) High interannual variability of sea ice thickness in the Arctic region. Nature 425:947–950

Lüpkes C, Gryanik VM, Hartmann J, Andreas EL (2012) A parametrization, based on sea ice morphology, of the neutral atmospheric drag coefficients for weather prediction and climate models. J Geophys Res 117:D13112

Makshtas AP, Shoutilin SV, Andreas EL (2003) Possible dynamic and thermal causes for the recent decrease in sea ice in the Arctic Basin. J Geophys Res 108(C7):3232

Meylan MH, Squire VA (1994) The response of ice floes to ocean waves. J Geophys Res 99:891–900

Perovich DK, Jones KF (2014) The seasonal evolution of sea ice floe size distribution. J Geophys Res 119:8767–8777

Roach LA, Horvat C, Dean SM, Bitz CM (2018) An emergent sea ice floe size distribution in a global coupled ocean-sea ice model. J Geophys Res Oceans 123:4322–4337

Roach LA, Bitz CM, Horvat C, Dean SM (2019) Advances in modelling interactions between sea ice and ocean surface waves. J Adv Model Earth Syst 11:4167–4181

Rosati A, Miyakoda K (1988) A general circulation model for upper ocean simulation. J Phys Oceanogr 18:1601–1622

Soh LK, Tsatsoulis C, Holt B (1998) Identifying ice floes and computing ice floe distributions in SAR images. In: Tsatsoulis C, Kwok R (eds) Analysis of SAR Data of the Polar Oceans. Springer Verlag, New York, pp 9–34

Squire VA (2007) Of ocean waves and sea ice revisited. Cold Reg Sci Technol 49:110–133

Squire VA, Dugan JP, Wadhams P, Rottier PJ, Liu AJ (1995) Of ocean waves and sea ice. Annu Rev Fluid Mech 27:115–168

Squire VA, Vaughan GL, Bennetts LG (2009) Ocean surface wave evolvement in the Arctic Basin. Geophys Res Lett 36:L22502

Stammerjohn S, Massom R, Rind D, Martinson D (2012) Regions of rapid sea ice change: An inter-hemispheric seasonal comparison. Geophys Res Lett 39:L06501

Steele M (1992) Sea ice melting and floe geometry in a simple ice-ocean model. J Geophys Res 97:17729–17738

Stubenrauch CJ, Rossow WB, Kinne S, Ackerman S, Cesana G, Chepfer H, Di Girolamo L, Getzewich B, Guignard A, Heidinger A, Maddux BC, Menzel WP, Minnis P, Pearl C, Platnick S, Poulsen C, Riedi J, Sun-Mack S, Walther A, Winker D, Zeng S, Zhao G (2013) Assessment of global cloud datasets from satellites: project and database initiated by the GEWEX radiation panel. Bull Amer Meteor Soc 94:1031–1049

Thorndike AS, Rothrock DA, Maykut GA, Colony R (1975) The thickness distribution of sea ice. J Geophys Res 80:4501–4513

Toyota T, Kohout A, Fraser AD (2016) Formation processes of sea ice floe size distribution in the interior pack and its relationship to the marginal ice zone off East Antarctica. Deep-Sea Res II Top Stud Oceanogr 131:28–40

Tsamados M, Feltham DL, Schroeder D, FloccoD FSL, Kurtz N, Laxon SW, Vihma T, Pirazzini R, Fer I et al (2014) Advances in understanding and parameterization of small-scale physical processes in the marine Arctic climate system: a review. Atmos Chem Phys 14:9403–9450

Williams TD, Bennetts LG, Squire VA, Dumont D, Bertino L (2013) Wave-ice interactions in the marginal ice zone. Part 1: Theoretical foundations. Ocean Model 7:81–91

WMO (2014) WMO sea-ice nomenclature, WMO/OMM/BMO - No.259 Edition 1970 - 2014, WMO

Zhang J, Lindsay R, Schweiger A, Rigor I (2012) Recent changes in the dynamic properties of declining Arctic sea ice: a model study. Geophys Res Lett 39:L20503

Zhang J, Schweiger A, Steele M, Stern H (2015) Sea ice floe size distribution in the marginal ice zone: Theory and numerical experiments. J Geophys Res Oceans 120:3484–3498

Zhang J, Stern H, Hwang B et al (2016) Modeling the seasonal evolution of the Arctic sea ice floe size distribution. Elem Sci Anth 4:126